antioxidants

MDPI

Article

ZDHHC22-Mediated AKT1 Palmitoylation Promotes Bile Acid-Induced Gastric Intestinal Metaplasia and Is Inhibited by Naringenin

Na Chen [1,†], Qijin He [1,†], Shuyang Xu [1,†], Zheng Rong [1], Ping Li [1], Shujun Gong [1], Huange Gao [1], Min Gao [1], Huiling Yu [2], Kui Jiang [1,*] and Jingwen Zhao [1,*]

[1] Department of Gastroenterology and Hepatology, Tianjin Medical University General Hospital, Tianjin Institute of Digestive Diseases, Tianjin Key Laboratory of Digestive Diseases, No. 154 Anshan Road, Tianjin 300052, China; chenna1995@tmu.edu.cn (N.C.); heqijin@tmu.edu.cn (Q.H.); xushuyang@tmu.edu.cn (S.X.)

[2] Department of Gastroenterology, Affiliated Hospital of Hebei University, Baoding 071000, China

* Correspondence: jiangkui@tmu.edu.cn (K.J.); jingwenzhao@tmu.edu.cn (J.Z.); Tel.: +86-13820812239 (K.J.); +86-15002233152 (J.Z.)

† These authors contributed equally to this work.

Abstract

Gastric intestinal metaplasia (GIM) is a premalignant lesion associated with bile reflux, but the molecular mechanisms linking bile acid exposure to metaplastic transformation remain incompletely understood. Although S-palmitoylation regulates protein signaling, its role in bile acid-induced gastric metaplasia remains unclear. Naringenin possesses gastroprotective and antioxidant properties; however, whether it influences bile acid-induced metaplastic changes has not been established. Here, the protective effects of naringenin and the potential involvement of ZDHHC22-associated AKT1 palmitoylation were investigated in deoxycholic acid (DCA)-exposed INS-GAS mice and GES-1 cells. Early naringenin intervention, initiated before overt histological evidence of GIM emerged, attenuated subsequent gastric histopathological alterations and reduced the expression of the intestinal metaplasia markers MUC2 and CDX2 in gastric tissues and GES-1 cells. Network pharmacology analysis prioritized AKT1 as a candidate molecular node, while human single-cell transcriptomic analyses characterized AKT1 expression across gastric disease states. Naringenin reduced AKT1 phosphorylation and attenuated DCA-induced oxidative stress and mitochondrial abnormalities. To explore the upstream mechanisms underlying these effects, integrated transcriptomic analysis identified ZDHHC22 as a candidate regulator of the response to naringenin, while single-cell analyses further implicated this palmitoyltransferase in the metaplastic response. IP-ABE assays showed that DCA exposure increased AKT1 palmitoylation. This modification was reduced by naringenin, the palmitoylation inhibitor 2-bromopalmitate (2-BP), or ZDHHC22 knockdown. Overexpression of wild-type ZDHHC22, but not of its catalytically inactive mutant, enhanced AKT1 palmitoylation, supporting a catalytic contribution of ZDHHC22 to this modification. Importantly, interventions that reduced AKT1 palmitoylation also decreased AKT1 phosphorylation, MUC2 and CDX2 expression, reactive oxygen species accumulation, and mitochondrial depolarization. These concordant effects suggest a regulatory relationship between AKT1 palmitoylation and phosphorylation and indicate that enhanced AKT1 palmitoylation may contribute to DCA-induced metaplastic changes and mitochondrial abnormalities. Collectively, these findings suggest that early naringenin

Academic Editors: Alessandra Napolitano and José Ángel Rufián-Henares

Received: 9 September 2026
Revised: 27 October 2026
Accepted: 16 November 2026
Published: 24 November 2026

Copyright: © 2026 by the author. Licensee MDPI, Basel, Switzerland. This article is an open access article distributed under the terms and conditions of the Creative Commons Attribution (CC BY) license.

intervention attenuates bile acid-associated metaplastic progression, potentially by modulating the ZDHHC22–AKT1 palmitoylation–phosphorylation axis.

Keywords: naringenin; intestinal metaplasia; palmitoylation; ZDHHC22

1. Introduction

Gastric intestinal metaplasia (GIM), a premalignant lesion characterized by the replacement of gastric mucosa with intestinal-type epithelium, represents a critical step in the pathogenesis of intestinal-type gastric cancer (GC). Although its molecular mechanisms remain incompletely defined, bile reflux has been established as an independent risk factor for GIM development [1]. Bile acids (BAs), key components of refluxate, activate nuclear and membrane receptors (e.g., FXR, GPBAR1) to drive aberrant differentiation [2,3], highlighting the need to elucidate BA-induced metaplastic mechanisms and identify therapeutic targets.

Protein palmitoylation, catalyzed by ZDHHC palmitoyltransferases, regulates substrate localization, stability, and interaction networks [4,5]. Dysregulated palmitoylation contributes to tumorigenesis; for example, Nrf2 palmitoylation enhances its stability and promotes antioxidant responses in GC [6]. Inhibition of specific ZDHHC enzymes impairs cancer progression [7–9], suggesting palmitoylation as a therapeutic target. However, the role of ZDHHC-mediated palmitoylation in GIM and its interaction with BA signaling remain unclear.

AKT1 activation has been implicated in GIM progression, with elevated phosphorylated AKT1 (p-AKT1) levels observed in patient samples [10] and functional studies suggesting a promotive role in metaplasia [11,12]. AKT1 signaling also intersects with inflammatory pathways [13], indicating a potential role in metaplastic transformation within a compromised mucosal microenvironment.

Primary studies have identified AKT1 S-palmitoylation as an additional regulatory modification. Blaustein et al. reported C344-associated palmitoylation and changes in AKT1 localization and phosphorylation following C344S substitution [14]. Bu et al. subsequently identified AKT1 palmitoylation at C77/C224 and implicated ZDHHC17/24 in its regulation in liver disease models [15]. These findings provide a rationale for investigating AKT1 palmitoylation in bile acid-induced GIM, while the relevant residues, regulatory enzymes, and functional consequences in gastric epithelial cells remain to be defined.

Naringenin is a naturally occurring citrus flavanone. A randomized single-ascending-dose trial in healthy adults reported oral systemic exposure and short-term tolerability of naringenin delivered in a whole-orange extract [16]. Preclinical studies have reported antioxidant [17], anti-inflammatory [18], and antitumor effects, including suppression of metastasis [19]. Naringenin has also been shown to attenuate oxidative stress and mitochondrial dysfunction in neuronal models [20] and to protect against ethanol-induced gastric mucosal injury in mice [21]. These findings provide a rationale for investigating naringenin in experimental bile acid-induced GIM, but do not establish its efficacy in preventing metaplastic progression.

In this study, we investigated the involvement of ZDHHC22-associated AKT1 palmitoylation in bile acid-induced GIM and its relationship with AKT1 phosphorylation and mitochondrial oxidative stress. We further examined whether naringenin modulates these molecular changes alongside its effects on metaplastic phenotypes. Our findings provide experimental support for a potential ZDHHC22–AKT1 regulatory mechanism in GIM, while the direct enzymatic relationship and the causal contribution of AKT1 palmitoylation require further investigation.

https://doi.org/10.3390/antiox15121549

2. Materials and Methods

2.1. Animals and Treatments

A total of 30 male SPF-grade INS-GAS mice (aged 8–12 weeks, weighing 30–32 g) were obtained from Hangzhou Ziyuan Experimental Animal Technology Co., Ltd. (Hangzhou, China) and housed under standard conditions. The mice were randomly assigned to four groups (n = 9 for CON and DCA groups; n = 6 for DCA+Nar-L and DCA+Nar-H groups). The CON group received purified water, while the DCA group was given 0.2% DCA (MedChemExpress, Monmouth Junction, NJ, USA) in drinking water. At 4 months, 3 mice from the CON and DCA groups were sacrificed for initial assessment. Naringenin (Aladdin, Shanghai, China) administration was subsequently initiated in the designated intervention groups at 10 or 20 mg/kg by intraperitoneal injection for two months. These dose levels were selected with reference to previous preclinical studies [21] to compare biological responses at two doses differing by twofold. The study was not designed to establish an optimal dose or a maximum tolerated dose. All remaining mice were euthanized at month 6 for endpoint analyses. The study was approved by the institutional animal ethics committee (IRM/2-IACUC-2407-002).

2.2. Network Pharmacology Analysis

Potential targets of naringenin were retrieved from the TCMSP and SwissTargetPrediction databases, while disease-related targets for "bile acid-induced intestinal metaplasia" were collected from GeneCards and OMIM, applying a Score >2 filter. The union of naringenin targets and disease targets was analyzed using the Venny 2.1.0 tool to identify common genes. These intersecting targets were imported into Cytoscape(version 3.9.1), and the cytoHubba plugin was used to rank genes by four algorithms (Degree, Closeness, MCC, and Betweenness). The final key targets were defined as the intersection of the top 10 genes from each ranking method. The identified common targets were uploaded to the Metascape database with species set to "Homo sapiens" for Gene Ontology (GO) and Kyoto Encyclopedia of Genes and Genomes (KEGG) enrichment analysis.

2.3. Cell Culture and Treatment

Human gastric epithelial GES-1 cells (Beijing Beina Chuanglian Biotechnology Research Institute, Beijing, China) were cultured in DMEM (Gibco, Thermo Fisher Scientific, Waltham, MA, USA) supplemented with 10% heat-inactivated fetal bovine serum (Vazyme, Nanjing, China) at 37 °C in a humidified atmosphere containing 5% CO_2. GES-1 cells were seeded into culture plates and cultured for 24 h before treatment. Subsequently, cells were exposed to DCA (100 μM) for 24 h. In the drug intervention groups, cells were pretreated with naringenin (10 or 20 μM, Aladdin), MK-2206 (5 μM, MedChemExpress, Monmouth Junction, NJ, USA), or 2-BP (25 μM, Merck, Darmstadt, Germany) for 2 h before DCA exposure; the indicated compounds remained present during the subsequent 24 h DCA exposure. The in vitro concentrations of naringenin were determined based on our preliminary cell viability screening, which confirmed no significant cytotoxicity within this range (Supplementary Figure S1). The concentrations of MK-2206 and 2-BP were selected based on established protocols from previous studies [22,23].

2.4. Western Blot

Protein lysates were prepared from gastric tissues or cells using lysis buffer supplemented with phosphatase inhibitor and PMSF (100:1; all reagents from Solarbio, Beijing, China). After centrifugation at 12,000 rpm for 10 min at 4 °C, the supernatant was collected, and protein concentration was determined by BCA assay (Solarbio, Beijing, China). Equal amounts of protein were separated by 7.5% SDS-PAGE and transferred to PVDF

membranes (Vazyme, Nanjing, China) at 400 mA for 40 min. The membranes were blocked with rapid blocking solution (Epizyme Biotech, Shanghai, China) for 15 min at room temperature, incubated with primary antibodies at 4 °C overnight, and then with HRP-conjugated secondary antibodies for 1 h at room temperature. After washing with TBST, protein bands were visualized using ECL reagents (Solarbio, Beijing, China) and quantified with ImageJ(version 1.53e). Antibody details are listed in Supplementary Table S1.

2.5. Immunoprecipitation Combined with Acyl-Biotin Exchange (IP-ABE)

Cultured cells grown in 10 cm dishes were lysed in 1 mL of RIPA lysis buffer supplemented with PMSF (RIPA: PMSF stock solution, 100:1, *v*/*v*), with one dish used to prepare each sample. Following centrifugation, the clarified supernatant was collected. For each immunoprecipitation reaction, approximately 1 mL of clarified lysate was incubated with 3 μL of anti-AKT1 rabbit monoclonal antibody (Cell Signaling Technology, Danvers, MA, USA; Cat. No. 2938T; approximately 1:333 dilution in RIPA lysate) overnight at 4 °C with gentle agitation. Subsequently, 40 μL of Protein A/G agarose bead suspension (Beyotime Biotechnology, Cat. No. P2055, Shanghai, China) was added, and the mixture was incubated for 2 h at room temperature. The bead-bound complexes were collected by centrifugation at 2500 rpm for 5 min and washed five times with RIPA buffer supplemented with PMSF at the same ratio.

The immunoprecipitated samples were then processed using the AIMSMASS Palmitoylation IP-ABE Kit (Aimsscientific, Shanghai, China; Cat. No. AM10314) according to the manufacturer's instructions. Matched hydroxylamine-treated (+HA) and hydroxylamine-omitted (−HA) samples were included for every treatment condition in each independent experiment. The −HA samples were processed in parallel without hydroxylamine to assess hydroxylamine-independent background labeling. Following the acyl–biotin exchange procedure, samples were subjected to SDS-PAGE and membrane transfer. Biotin-labeled proteins were detected using the streptavidin–HRP supplied with the kit, diluted 1:5000 in Tris-buffered saline containing Tween 20 (TBST). Three independent biological experiments were performed (n = 3). For quantification, the Palm signal in each +HA sample was normalized to the corresponding AKT1 signal in the immunoprecipitated material.

2.6. qRT-PCR

Total RNA was extracted from gastric cells using Trizol reagent (Vazyme, Nanjing, China). cDNA was synthesized from 1000 ng of RNA using HiScript qRT SuperMix II (Vazyme, Nanjing, China). Quantitative PCR was performed in 20 μL reactions containing 0.5 μL cDNA, 0.4 μL of each primer, and 10 μL ChamQ SYBR qPCR Master Mix (Vazyme, Nanjing, China). The thermal cycling conditions were: 95 °C for 30 s, followed by 40 cycles of 95 °C for 10 s and 60 °C for 30 s, with subsequent melting curve analysis. Relative mRNA expression levels were calculated using the $2^{-\Delta\Delta C_T}$ method. Primer sequences are listed in Supplementary Table S2.

2.7. Statistical Analysis

Data statistical analysis was performed using GraphPad Prism 9.0 software. Normally distributed data are presented as the mean ± SEM. Two groups were compared using a t-test, and three or more groups were analyzed using one-way analysis of variance (ANOVA). A p-value less than 0.05 was considered statistically significant.

2.8. Additional Experimental Procedures

Detailed experimental procedures, including fluorescence probe assays, transmission electron microscopy (TEM), single-cell RNA sequencing, and transcriptome sequencing, are provided in the Supplementary Materials.

3. Results

3.1. Naringenin Attenuates DCA-Induced Gastric Histological Changes and IM-Associated Marker Expression

The INS-GAS mouse model was used to evaluate the effects of naringenin initiated during an early stage of DCA-induced gastric changes (Figure 1A). After four months of DCA exposure, gastric MUC2 expression was increased in the sampled DCA-treated mice (Figure 1B), whereas typical histological features of intestinal metaplasia were not evident in the examined sections (Figure 1C). We therefore considered this time point an early marker-positive state, provisionally described as a pre-metaplastic stage, rather than histologically established GIM. Naringenin administration was initiated at this time point to examine its effects on the subsequent development of DCA-associated gastric changes. After 2 months of intervention, the DCA group exhibited significant typical IM changes, such as atrophy of the superficial epithelium of the gastric mucosa, disordered tissue structure, and goblet cell metaplasia of glands. Representative goblet cells and disorganized glandular architecture in the DCA group are indicated by red and blue arrows, respectively, in Figure 1D. In contrast, the degree of IM in the naringenin intervention groups (especially the high-dose group) was significantly reduced, showing a dose-dependent improvement trend (Figure 1D). Furthermore, the expressions of CDX2 and MUC2 proteins in the DCA group were significantly increased, while naringenin intervention reduced the expressions of these markers, and the inhibitory effect of high-dose naringenin was more significant (Figure 1E–G).

To verify the intervention effect of naringenin on bile acid-induced IM in an in vitro model, this study established an in vitro IM model by stimulating GES-1 cells with DCA. The expression of IM markers was verified at both gene and protein levels. The results (Figure 2A–F) showed that DCA stimulation significantly increased the mRNA and protein expression levels of MUC2 and CDX2, while the mRNA and protein expression in the naringenin intervention groups was significantly decreased, with the high-dose group showing a stronger inhibitory effect. Together, these findings show that naringenin attenuated gastric histological changes at the experimental endpoint and reduced DCA-induced IM-associated marker expression in gastric tissues and GES-1 cells. Because naringenin administration began before typical histological IM was evident, these results are consistent with an early preventive effect within this experimental model rather than reversal of established GIM.

3.2. Integrative Analyses Identify AKT1 as a Candidate Molecular Node in Bile Acid-Induced IM

To prioritize candidate molecular targets for experimental investigation, network pharmacology analysis was performed. Target genes of naringenin were acquired from TCMSP and SwissTargetPrediction databases, normalized via UniProt, yielding 149 unique targets. Disease-related genes for bile acid-induced IM were retrieved from GeneCards and OMIM, resulting in 828 targets after merging. Venn analysis identified 51 overlapping genes between naringenin and metaplasia targets (Figure 3A,B). These overlapping genes were imported into Cytoscape and analyzed using the cytoHubba plugin with four algorithms (Degree, Closeness, MCC, Betweenness). Intersection of the top 10 genes from each method identified 8 key targets, with AKT1 exhibiting the highest average rank, supporting its prioritization as a candidate for subsequent experimental investigation (Figure 3C,D).

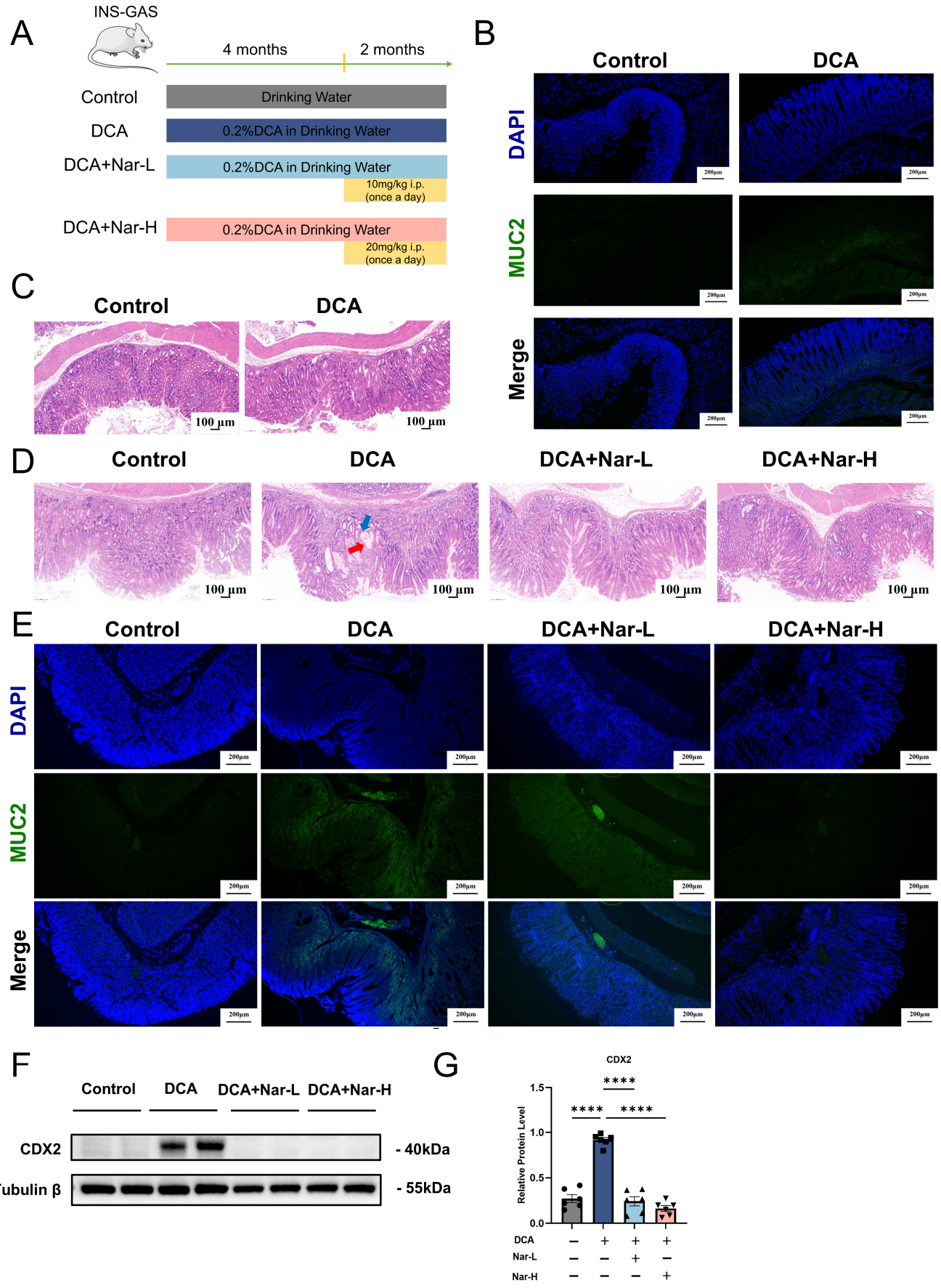


Figure 1. Naringenin intervention reduces the expression of IM markers in mouse models: (**A**) Experimental timeline and treatment groups. (**B**) MUC2 immunofluorescence and (**C**) H&E staining

of gastric tissues after 4 months of bile acid intervention. (**D**) H&E staining and (**E**) MUC2 immunofluorescence after 2 months of naringenin treatment. (**F**) Representative Western blot and (**G**) quantitative analysis of CDX2 protein expression. In panel (**D**), red arrows indicate goblet cells, and blue arrows indicate disorganized glandular architecture in the DCA group. Scale bars: 200 μm (**B**,**E**), 100 μm (**C**,**D**). **** $p < 0.0001$

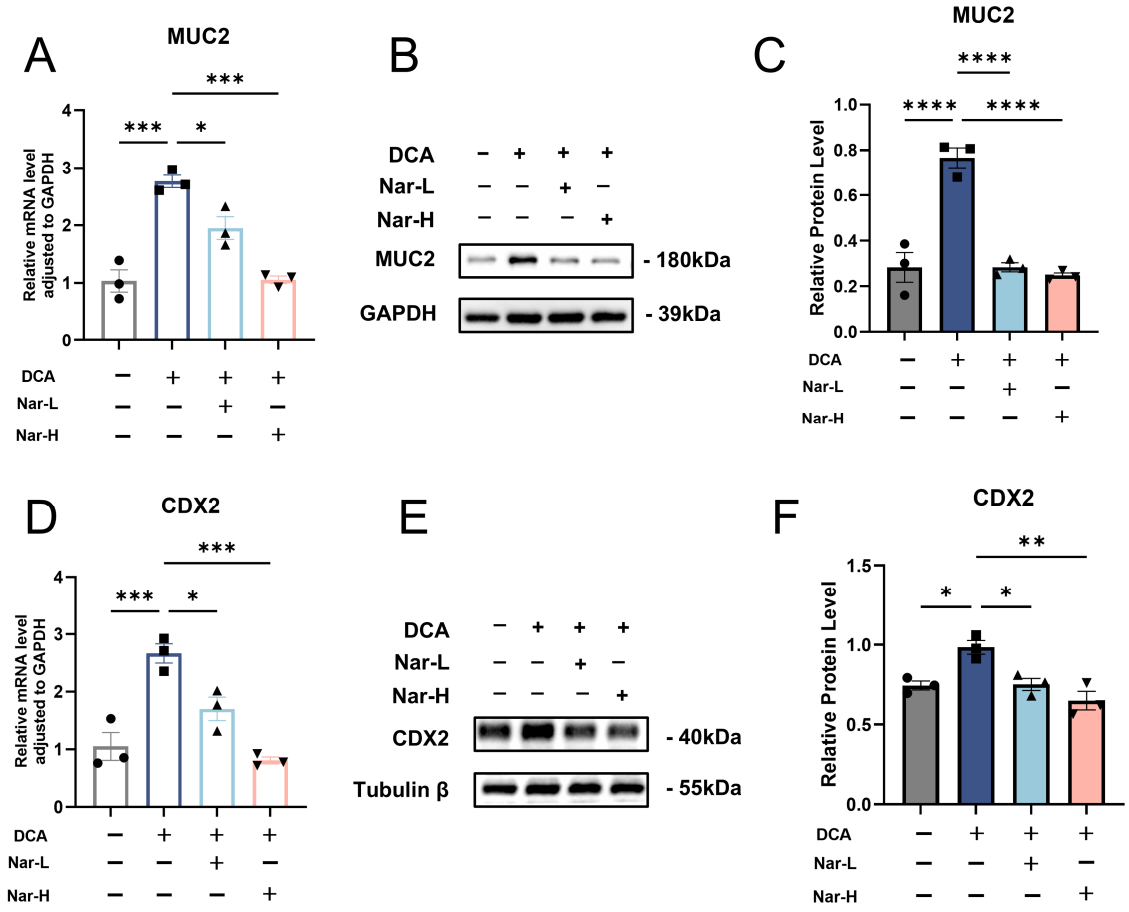


Figure 2. Naringenin intervention reduces the expression of IM markers in cell models: (**A**) MUC2 mRNA expression. (**B**) Representative MUC2 protein blot. (**C**) Quantitative analysis of MUC2 protein levels. (**D**) CDX2 mRNA expression. (**E**) Representative CDX2 protein blot. (**F**) Quantitative analysis of CDX2 protein levels. * $p < 0.05$, ** $p < 0.01$, *** $p < 0.001$, **** $p < 0.0001$.

To examine AKT1 expression across gastric disease states, single-cell RNA-seq data from Gene Expression Omnibus (GEO) (GSE134520; including CAG, NAG, IM, and EGC samples) were analyzed. Cluster analysis demonstrated that AKT1 expression was most elevated in IM samples, moderately expressed in chronic atrophic gastritis (CAG), and lowest in non-atrophic gastritis (NAG), indicating differences in AKT1 expression across the sampled gastric disease states (Figure 3E–G).

Analysis of TCGA-STAD data showed higher AKT1 expression in gastric adenocarcinoma than in normal samples. Within the clinicopathological categories examined, the highest expression levels were observed in stage I, grade 2, and N0 tumors, respectively (Figure 3H). These observations describe AKT1 expression in a gastric cancer cohort.

Together, these analyses prioritized AKT1 for experimental investigation and linked its expression to the sampled gastric disease states.

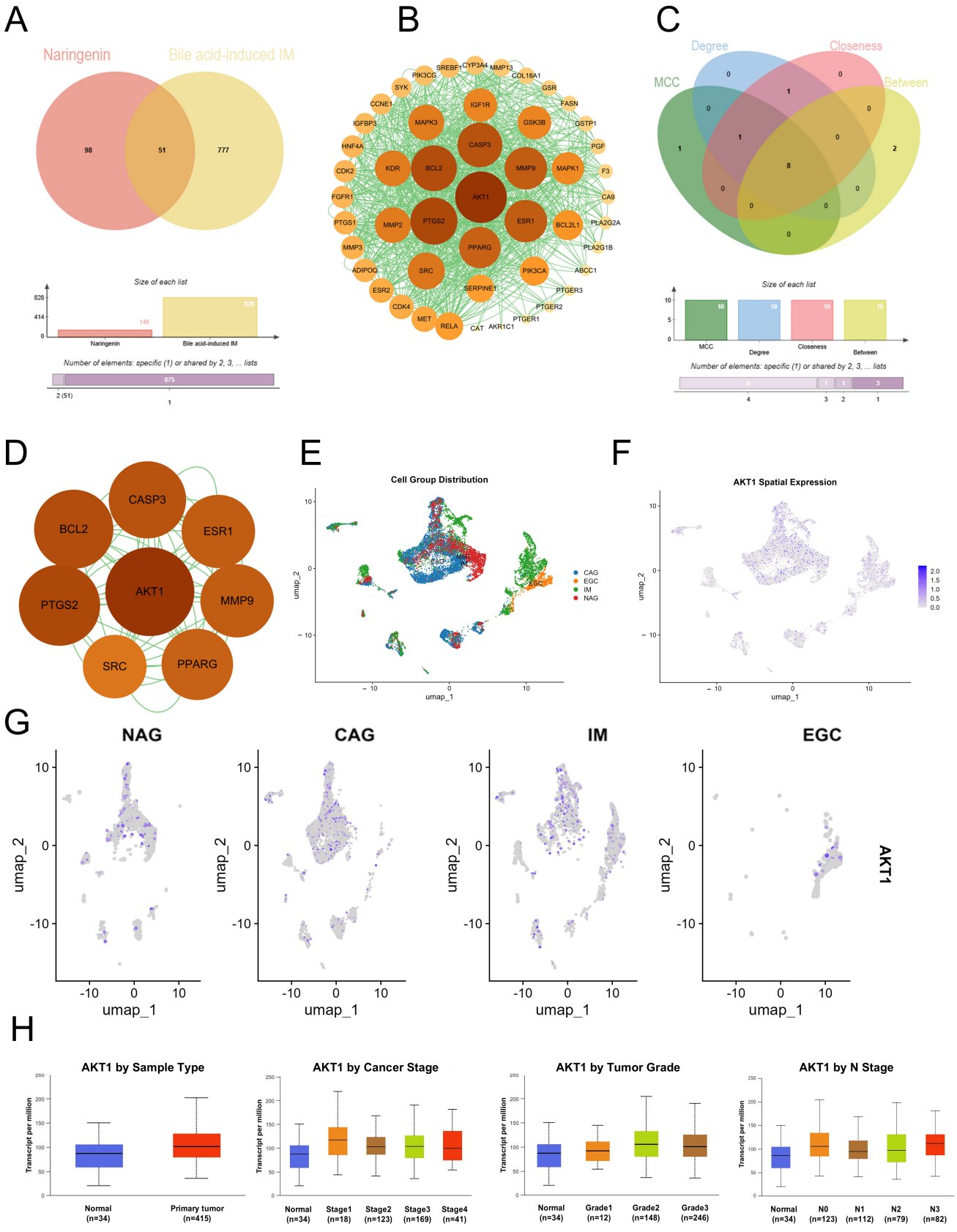


Figure 3. Integrative analyses identify AKT1 as a candidate molecular node in bile acid-induced IM: (**A**) Venn diagram of overlapping targets between naringenin and bile acid-induced IM. (**B**) Protein–protein interaction (PPI) network of common targets. (**C**,**D**) Hub target screening using cytoHubba algorithms. (**E**–**G**) Single-cell RNA-seq analysis: (**E**) UMAP visualization of cell populations from

NAG, CAG, IM, and EGC samples; (**F**) AKT1 expression gradient mapped onto UMAP space; (**G**) layered display of cell populations and AKT1 expression. (**H**) AKT1 expression levels across sample types, tumor stages, grades, and nodal metastasis status in the TCGA-STAD cohort.

3.3. Naringenin Reduces AKT1 Phosphorylation, and AKT Inhibition Attenuates DCA-Induced IM Marker Expression

To examine whether naringenin treatment is associated with changes in AKT1 phosphorylation, we assessed p-AKT1 and total AKT1 levels in gastric tissues and DCA-treated GES-1 cells. In the animal model, the protein expression of phosphorylated AKT1 (p-AKT1) in the gastric tissue of mice in the DCA group was significantly higher than that in the control group, while the total AKT1 protein level showed no significant change. After naringenin intervention, the protein expression of p-AKT1 decreased significantly, with a more obvious decrease in the high-dose group (Figure 4A,B). In the DCA-induced GES-1 cell model, the p-AKT1 protein level was higher than that in the control group, while naringenin intervention could reduce the p-AKT1 protein expression level, and the intervention effect of high-concentration naringenin was more significant (Figure 4C,D).

To examine the contribution of AKT signaling to DCA-induced IM marker expression, we treated GES-1 cells with the pharmacological AKT inhibitor MK-2206. The results showed that MK-2206 treatment reduced the p-AKT1 protein expression level in DCA-stimulated GES-1 cells, while the AKT1 protein expression showed no obvious change (Figure 4G,H). At the same time, it could also significantly downregulate the mRNA and protein expression levels of IM markers MUC2 and CDX2 (Figure 4E–G,I,J). These results support the involvement of AKT signaling in DCA-induced IM marker expression and show that naringenin reduces AKT1 phosphorylation.

3.4. Effects of Naringenin and AKT Inhibition on DCA-Induced Oxidative Stress and Mitochondrial Abnormalities

GO and KEGG pathway enrichment analyses of the 8 core targets identified by network pharmacology revealed significant enrichment in oxidative stress-related processes. GO analysis highlighted biological processes including “negative regulation of intracellular signal transduction”, “response to decreased oxygen levels”, “response to reactive oxygen species”, and “negative regulation of the intrinsic apoptotic signaling pathway” (Figure 5A). KEGG analysis showed enrichment in “lipid and atherosclerosis”, “signaling pathways in cancer”, and “estrogen signaling pathway” (Figure 5B). These enrichment results motivated further assessment of oxidative stress and mitochondrial phenotypes following naringenin treatment or pharmacological AKT inhibition.

Evaluation of mitochondrial oxidative stress using MitoSOX Red and DCFH-DA probes demonstrated that DCA exposure increased DCFH-DA-derived and MitoSOX Red fluorescence signals compared with controls. Pretreatment with either naringenin or MK-2206 attenuated these increases (Figure 5C,D).

JC-1 probe analysis of mitochondrial membrane potential ($\Delta\Psi m$) revealed a significant decrease in the red/green fluorescence ratio following DCA exposure, indicating mitochondrial depolarization. Both naringenin and MK-2206 pretreatment prevented this loss of $\Delta\Psi m$, again with high-dose naringenin showing effects similar to MK-2206 (Figure 5E,F).

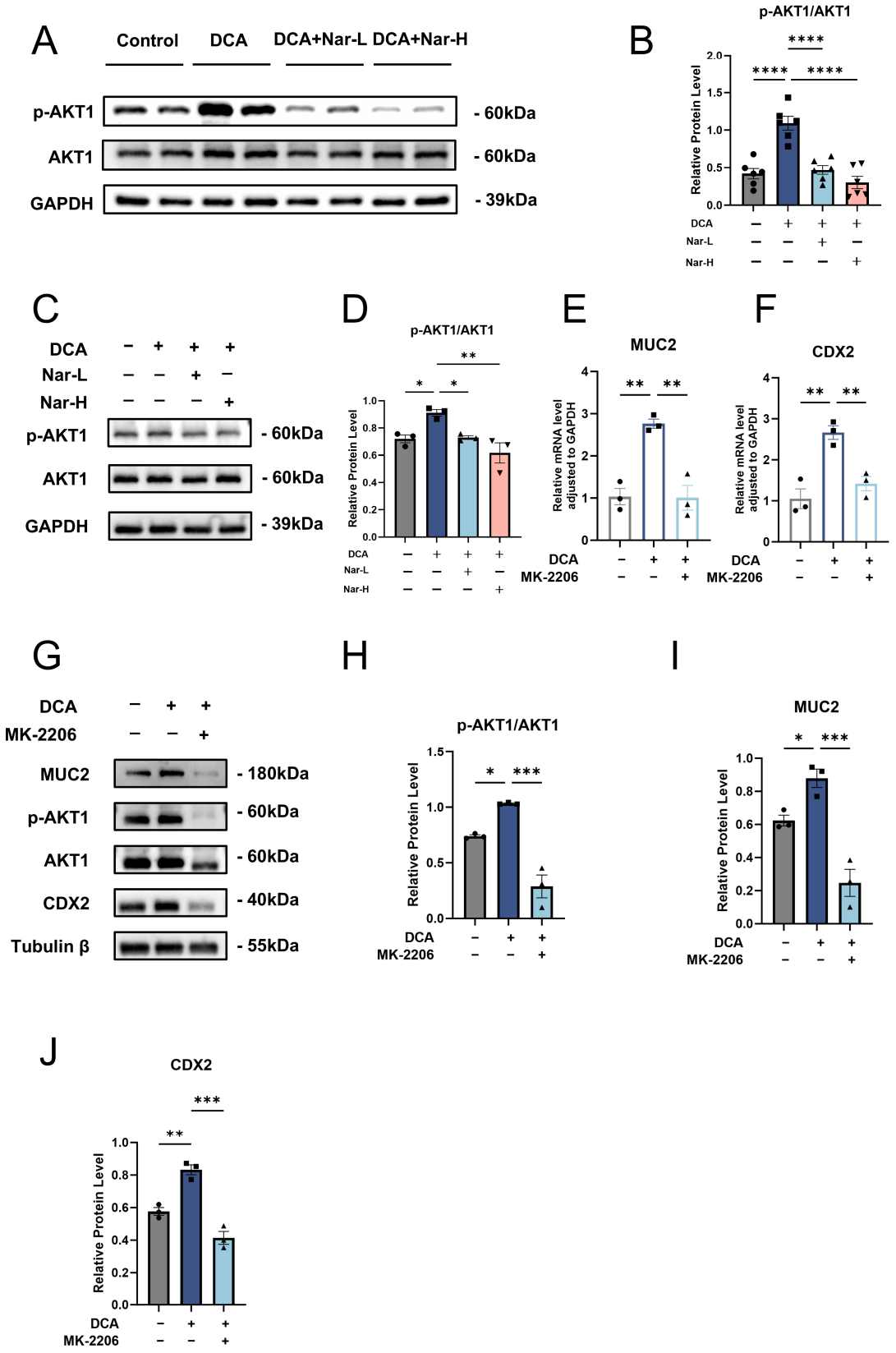


Figure 4. Naringenin reduces AKT1 phosphorylation, and AKT inhibition attenuates DCA-induced IM marker expression: (**A**) Representative Western blot of p-AKT1 and AKT1 protein expression in mouse gastric tissue following naringenin intervention. (**B**) Quantitative analysis of p-AKT1/AKT1 protein expression shown in (**A**). (**C**) Representative Western blot of p-AKT1 and AKT1 protein expression in the cellular IM model following naringenin intervention. (**D**) Quantitative analysis of

p-AKT1/AKT1 protein expression shown in (**C**). (**E**) MUC2 mRNA expression levels in the cellular IM model following MK-2206 treatment. (**F**) CDX2 mRNA expression levels in the cellular IM model following MK-2206 treatment. (**G**) Representative Western blot of MUC2, p-AKT1, AKT1, and CDX2 protein expression in the cellular IM model following MK-2206 treatment. (**H**) Quantitative analysis of p-AKT1/AKT1 protein expression shown in (**G**). (**I**) Quantitative analysis of MUC2 protein expression shown in (**G**). (**J**) Quantitative analysis of CDX2 protein expression shown in (**G**). * $p < 0.05$, ** $p < 0.01$, *** $p < 0.001$, **** $p < 0.0001$.

Transmission electron microscopy examination revealed mitochondrial ultrastructural abnormalities in DCA-exposed GES-1 cells and mouse gastric tissues, including vacuolization and cristae damage. These abnormalities were less pronounced following naringenin treatment (Figure 5G,H). Blue arrows in Figure 5G,H highlight representative mitochondria and their cristae morphology to facilitate comparison of damaged and relatively preserved ultrastructural features across the groups.

Naringenin and MK-2206 attenuated DCA-induced oxidative stress and mitochondrial depolarization. Naringenin also preserved mitochondrial ultrastructure. These findings link reduced AKT signaling to improved mitochondrial phenotypes in this model, without resolving the direction of this relationship.

3.5. ZDHHC22 Knockdown and Palmitoylation Inhibition Reduce DCA-Induced IM Marker Expression

To identify candidate genes associated with the response to naringenin, transcriptome sequencing was performed. A total of 19 differentially expressed genes were identified following naringenin treatment, including 11 upregulated and 8 downregulated genes. ZDHHC22 was selected for further investigation based on its differential expression and its role as a palmitoyltransferase (Figure 6A).

To validate the clinical relevance of ZDHHC22, single-cell RNA sequencing data from human gastric lesions were analyzed. ZDHHC22 expression was markedly elevated in CAG and IM samples, with high-expression regions precisely colocalizing with these pathological cell populations in UMAP space (Figure 6B–D), suggesting its potential role in metaplasia development.

To assess the contribution of ZDHHC22 to DCA-induced IM marker expression, we performed siRNA-mediated ZDHHC22 knockdown in GES-1 cells. Cells transfected with the scrambled siRNA (NC) were used as the negative control in all subsequent knockdown experiments. While DCA stimulation significantly increased protein levels of IM markers MUC2 and CDX2, ZDHHC22 silencing effectively suppressed their expression (Figure 6E–I). These findings support a contribution of ZDHHC22 to DCA-induced IM marker expression.

Given the palmitoyltransferase function of ZDHHC22, we next examined the effects of pharmacological palmitoylation inhibition. Treatment with 2-BP reduced MUC2 and CDX2 expression in DCA-exposed cells, resembling the effects of ZDHHC22 knockdown (Figure 6J–M). These findings support further investigation of palmitoylation-related processes in DCA-induced IM marker expression.

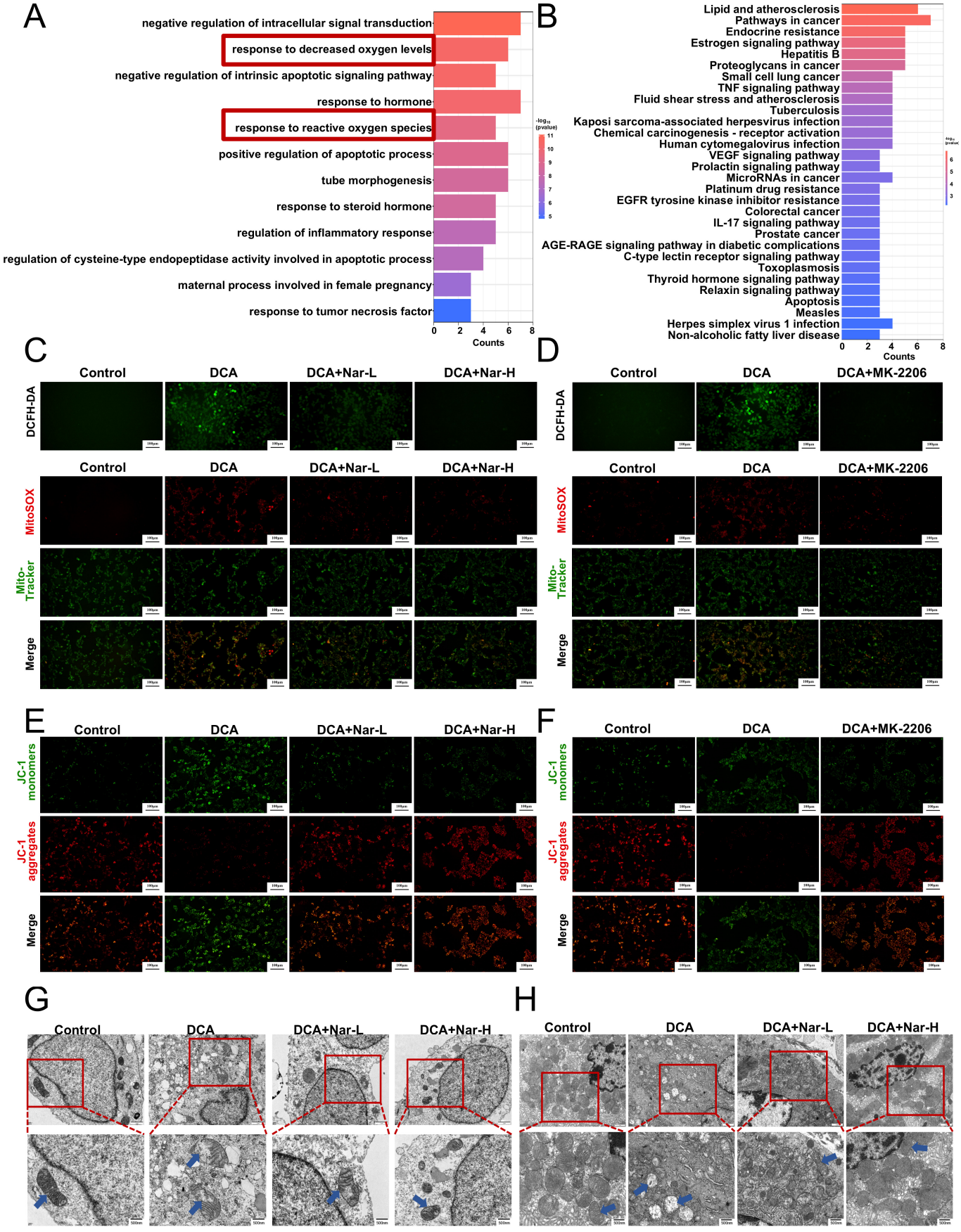


Figure 5. Naringenin and AKT inhibition attenuate DCA-induced oxidative stress and mitochondrial depolarization: (**A**) GO enrichment analysis of core targets. (**B**) KEGG pathway enrichment

https://doi.org/10.3390/antiox15121549

analysis. (**C**) Intracellular ROS (DCFH-DA) and mitochondrial ROS (MitoSOX Red/MitoTracker Green) levels with naringenin treatment. (**D**) Intracellular and mitochondrial ROS levels with MK-2206 treatment. (**E**) Mitochondrial membrane potential (JC-1) with naringenin. (**F**) Mitochondrial membrane potential with MK-2206. (**G**) Mitochondrial ultrastructure in cells by TEM. (**H**) Mitochondrial ultrastructure in gastric tissues by TEM. In panels (**G**,**H**), blue arrows highlight representative mitochondria and their cristae morphology across the groups, illustrating ultrastructural abnormalities, including vacuolization and cristae disruption, in the DCA group and relatively preserved mitochondrial structures in the control and naringenin-treated groups. Scale bars: 100 μm (**C**–**F**), 1 μm (upper panels in **G**,**H**), 500 nm (lower panels in **G**,**H**). In panel (A), red boxes highlight selected GO terms. In panels (G,H), red boxes indicate the regions shown at higher magnification in the lower images, with dashed lines connecting the corresponding areas.

3.6. ZDHHC22 Regulates AKT1 Palmitoylation, and Its Knockdown Attenuates DCA-Induced Mitochondrial Abnormalities

To investigate the functional relationship between ZDHHC22 and AKT1, we analyzed RNA-seq data from the TCGA-STAD cohort. Spearman correlation analysis revealed a significant positive correlation between ZDHHC22 expression and PI3K-AKT pathway activity (Figure 7A), suggesting a potential regulatory connection.

Using IP-ABE technology with parallel HA+ and HA− controls to verify signal specificity, we detected a specific AKT1 palmitoylation signal in DCA-induced metaplastic cells (Figure 7B,C), indicating that AKT1 is palmitoylated in this context. Subsequent analysis under various interventions showed that DCA stimulation significantly increased AKT1 palmitoylation compared to controls. This effect was markedly suppressed by the palmitoylation inhibitor 2-BP, ZDHHC22 knockdown, and naringenin treatment (Figure 7D,E).

To test the specificity of the knockdown effect, we re-expressed siRNA-resistant Syn-ZDHHC22 in ZDHHC22-depleted cells. Syn-ZDHHC22 restored the AKT1 palmitoylation signal under DCA stimulation (Figure 7F,G). Wild-type ZDHHC22 also increased AKT1 palmitoylation, whereas the DHHS mutant did not produce a comparable increase (Figure 7H,I). Together, these complementary experiments support ZDHHC22-dependent regulation of AKT1 palmitoylation and implicate its catalytic activity in this process.

We next investigated whether targeting ZDHHC22 or palmitoylation activity similarly protects against DCA-induced mitochondrial impairment. Mitochondrial ROS, intracellular ROS, and mitochondrial membrane potential were examined following ZDHHC22 knockdown or 2-BP treatment. Fluorescent analyses revealed that the DCA-induced elevation of both mitochondrial and intracellular ROS was substantially attenuated by either 2-BP treatment or ZDHHC22 knockdown (Figure 8A,B). Furthermore, JC-1 staining demonstrated that the DCA-induced mitochondrial membrane depolarization was markedly prevented by both interventions (Figure 8C).

Together, these results indicate that, similar to the protective effects of AKT inhibition and naringenin, ZDHHC22 knockdown or palmitoylation inhibition attenuates DCA-induced mitochondrial abnormalities and reduces AKT1 palmitoylation.

ZDHHC22 knockdown thus reduced AKT1 palmitoylation and improved mitochondrial readouts in DCA-exposed cells. Naringenin produced similar changes, linking its protective effects to modulation of these molecular and cellular responses.

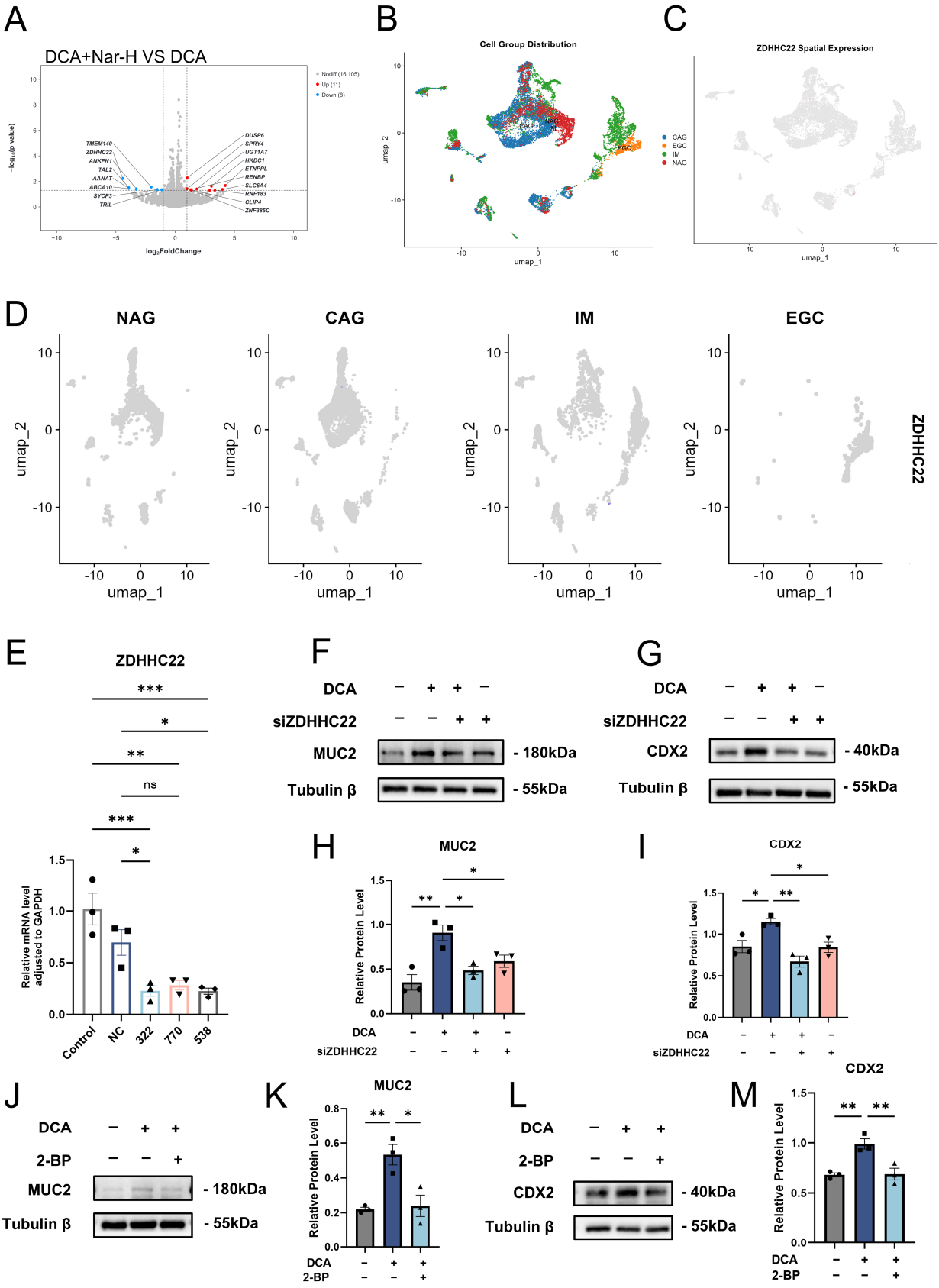


Figure 6. ZDHHC22 knockdown and pharmacological inhibition of palmitoylation reduce DCA-induced IM marker expression: (**A**) Volcano plot of differentially expressed genes from transcriptome sequencing. (**B**) UMAP visualization of cell populations (NAG, CAG, IM, EGC). (**C**) ZDHHC22 expression gradient in UMAP space. (**D**) Integrated display of cell populations and ZDHHC22 expression. (**E**) ZDHHC22 mRNA levels after siRNA transfection. (**F**) Representative MUC2 Western

blot after ZDHHC22 knockdown. (**G**) Representative CDX2 Western blot after ZDHHC22 knockdown. (**H**) Quantitative analysis of MUC2 protein after ZDHHC22 knockdown. (**I**) Quantitative analysis of CDX2 protein after ZDHHC22 knockdown. (**J**) Representative MUC2 Western blot after 2-BP treatment. (**K**) Quantitative analysis of MUC2 protein after 2-BP treatment. (**L**) Representative CDX2 Western blot after 2-BP treatment. (**M**) Quantitative analysis of CDX2 protein after 2-BP treatment. (Note: In all knockdown experiments, the control groups indicated by 'siZDHHC22-' represent cells transfected with the scrambled siRNA negative control (NC).) * $p < 0.05$, ** $p < 0.01$, *** $p < 0.001$.

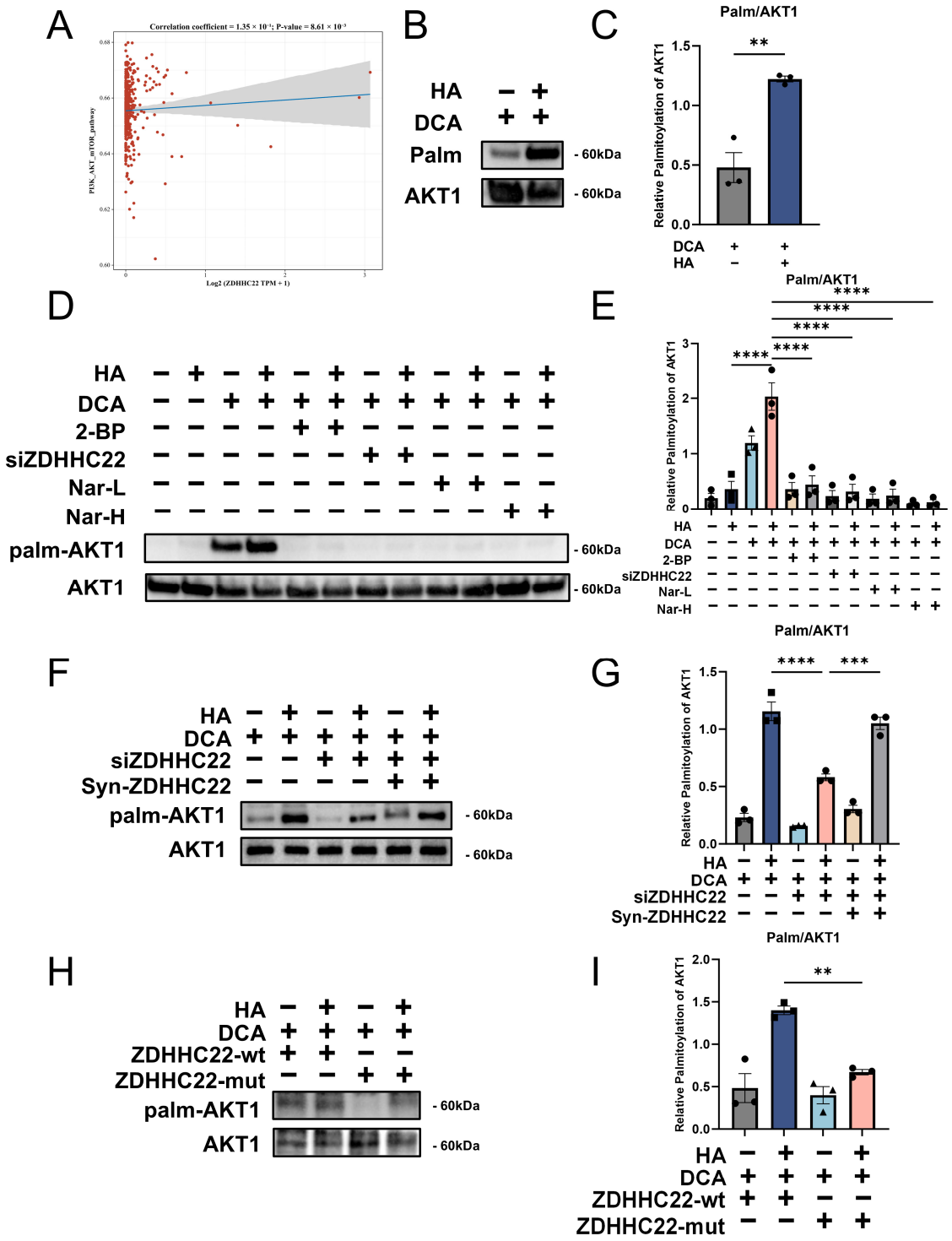
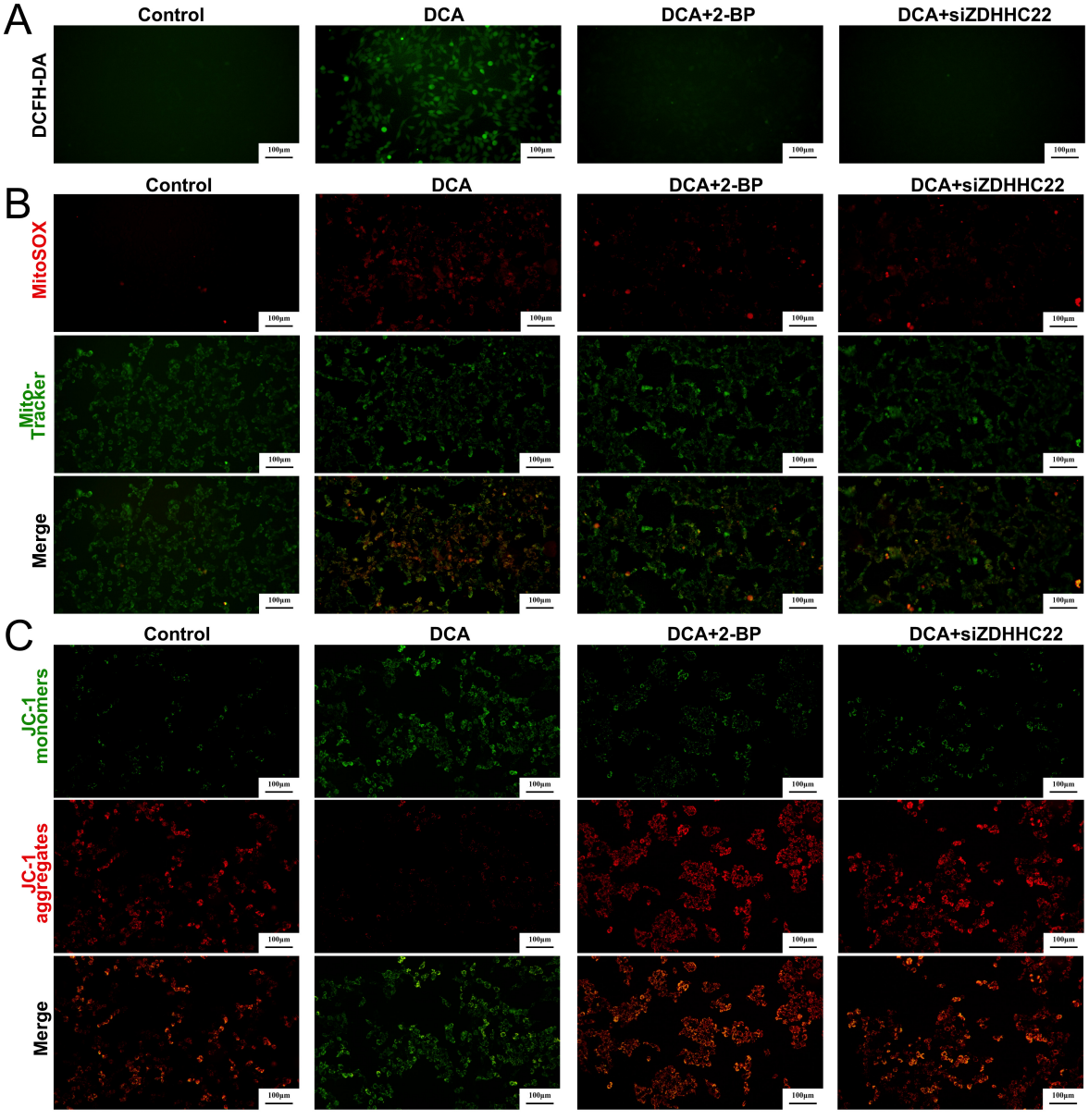


Figure 7. ZDHHC22 regulates AKT1 palmitoylation: effects of knockdown, rescue, and wild-type versus DHHS mutant expression: (**A**) Correlation between ZDHHC22 expression and PI3K-AKT

pathway activity in STAD. (**B**) AKT1 palmitoylation in DCA-induced metaplastic cells, as detected by IP-ABE assay with HA+ and HA− controls. (**C**) Quantification of the AKT1 palmitoylation signal in (**B**). (**D**) Representative IP-ABE Western blot of AKT1 palmitoylation following treatment with 2-BP, ZDHHC22 knockdown (siZDHHC22), and naringenin (Nar-L, Nar-H) under DCA stimulation. (**E**) Quantitative analysis of relative AKT1 palmitoylation shown in (**D**). (**F**) Representative IP-ABE Western blot demonstrating the rescue of AKT1 palmitoylation by co-transfection with the siRNA-resistant synonymous ZDHHC22 plasmid (Syn-ZDHHC22) in ZDHHC22-knockdown cells under DCA stimulation. (**G**) Quantitative analysis of relative AKT1 palmitoylation shown in (**F**). (**H**) Representative IP-ABE Western blot of AKT1 palmitoylation following transfection with wild-type ZDHHC22 (ZDHHC22-wt) or the catalytically inactive mutant (ZDHHC22-mut) under DCA stimulation. (**I**) Quantitative analysis of relative AKT1 palmitoylation shown in (H). ** $p < 0.01$, *** $p < 0.001$, **** $p < 0.0001$. Matched hydroxylamine-treated (+HA) and hydroxylamine-omitted (−HA) controls were included for every treatment condition in each independent experiment. For quantification, the Palm signal in each +HA sample was normalized to the corresponding immunoprecipitated AKT1 signal. IP-ABE experiments were performed in three independent biological replicates ($n = 3$).



https://doi.org/10.3390/antiox15121549

Figure 8. ZDHHC22 knockdown and palmitoylation inhibition attenuate DCA-induced mitochondrial dysfunction: (**A**) Intracellular ROS levels after 2-BP treatment or ZDHHC22 knockdown. (**B**) Mitochondrial ROS levels after 2-BP treatment or ZDHHC22 knockdown. (**C**) Mitochondrial membrane potential after 2-BP treatment or ZDHHC22 knockdown. Scale bars: 100 μm (**A**–**C**).

3.7. ZDHHC22 Knockdown and 2-BP Treatment Are Associated with Reduced AKT1 Phosphorylation

Given that S-palmitoylation regulates kinase membrane recruitment and subsequent activation, the potential interplay between AKT1 palmitoylation and its phosphorylation was next investigated. Specifically, phosphorylated AKT1 levels were assessed following 2-BP treatment or ZDHHC22 knockdown. Both 2-BP treatment and ZDHHC22 knockdown reduced phosphorylated AKT1 levels in DCA-exposed cells (Figure 9A–D), accompanying the reductions in AKT1 palmitoylation observed earlier. These results indicate a positive regulatory link between ZDHHC22-mediated palmitoylation and AKT1 phosphorylation.

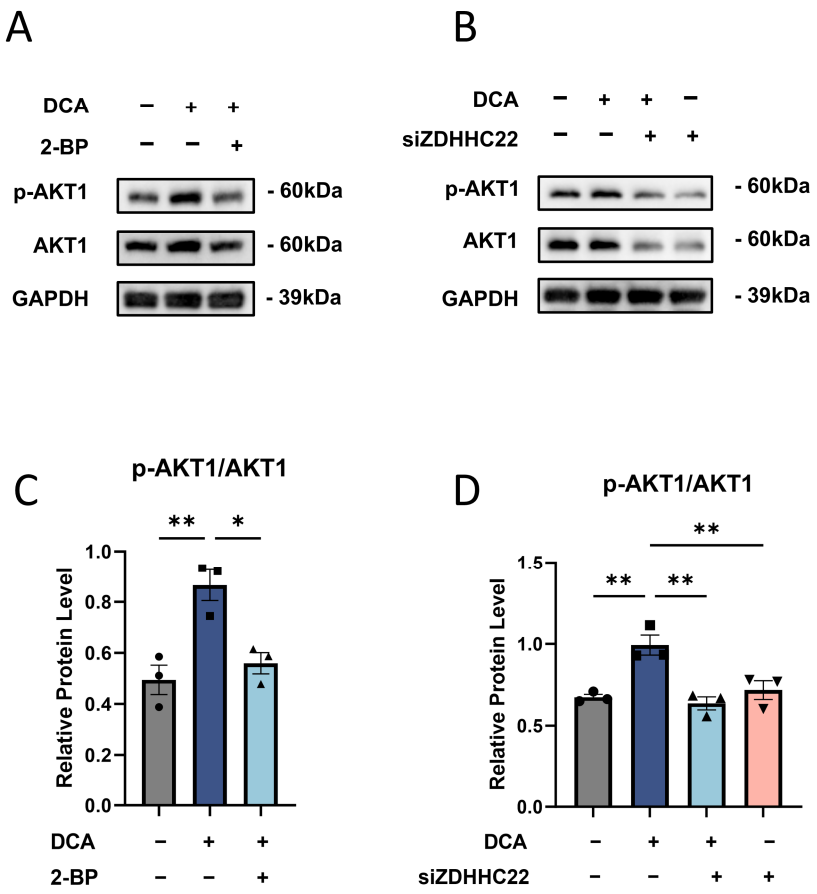


Figure 9. Effects of 2-BP treatment and ZDHHC22 knockdown on AKT1 phosphorylation: (**A**) Representative Western blot of p-AKT1/AKT1 levels after 2-BP treatment. (**B**) Representative Western blot of p-AKT1/AKT1 levels after ZDHHC22 knockdown. (**C**) Quantitative analysis of p-AKT1/AKT1 levels shown in (**A**). (**D**) Quantitative analysis of p-AKT1/AKT1 levels shown in (**B**). * $p < 0.05$, ** $p < 0.01$.

4. Discussion

In this study, we investigated the involvement of ZDHHC22-mediated AKT1 palmitoylation in bile acid-induced gastric intestinal metaplasia and evaluated the effects of early naringenin intervention. Our findings provide convergent evidence that ZDHHC22 contributes to the regulation of AKT1 palmitoylation in DCA stimulation. ZDHHC22 inhibition

reduced AKT1 palmitoylation and phosphorylation, decreased MUC2 and CDX2 expression, and alleviated oxidative stress and mitochondrial dysfunction. Naringenin produced a similar pattern of molecular and phenotypic effects and attenuated subsequent gastric histological changes when administered before histological GIM had developed. Together, these findings extend the study of AKT1 palmitoylation to gastric epithelial responses to bile acid exposure and identify ZDHHC22 as a candidate regulator of this process.

AKT signaling has been implicated in gastric carcinogenesis and metaplastic changes [10,11]. Consistent with these observations, DCA exposure increased AKT1 phosphorylation without substantially altering total AKT1 protein levels in our experimental models, suggesting that the response primarily involved AKT1 activation rather than increased protein abundance. Pharmacological inhibition of AKT with MK-2206 reduced DCA-induced MUC2 and CDX2 expression, supporting a functional contribution of AKT signaling to the expression of these metaplasia-associated markers. MK-2206 also attenuated intracellular and mitochondrial ROS accumulation and mitochondrial depolarization, suggesting that AKT signaling is associated with both metaplasia-associated marker expression and mitochondrial redox abnormalities. In addition, human single-cell transcriptomic analyses revealed differences in AKT1 expression among samples from non-atrophic gastritis, chronic atrophic gastritis, intestinal metaplasia, and early gastric cancer. Although these human datasets are descriptive and do not establish a causal role for AKT1 in disease progression, they provide relevant pathological context for our experimental findings.

Protein S-palmitoylation is a reversible lipid modification that regulates protein localization, stability, trafficking, and protein–protein interactions [4,5]. Previous studies have identified AKT1 as an S-palmitoylated protein. Blaustein et al. reported that AKT1 palmitoylation involving Cys344 influenced its subcellular localization and phosphorylation, while Bu et al. identified Cys77 and Cys224 as additional AKT1 palmitoylation sites and implicated ZDHHC17 and ZDHHC24 in AKT1 regulation in models of liver disease [14,15]. Our study extends these observations to gastric epithelial cells and a bile acid-induced injury model. We detected an AKT1-associated palmitoylation signal in gastric epithelial cells, which increased following DCA exposure. This signal was reduced by ZDHHC22 knockdown and by expression of the catalytically inactive ZDHHC22 mutant, whereas wild-type ZDHHC22 enhanced it. These findings provide complementary evidence that ZDHHC22 contributes to the regulation of AKT1 palmitoylation and that its catalytic activity is involved in this process.

The effects of ZDHHC22 are likely to depend on its available substrates and the signaling environment of a given cell type. ZDHHC22 has been reported to regulate the palmitoylation and cell-surface expression of calcium-activated potassium channels [24]. In breast cancer models, ZDHHC22-mediated mTOR palmitoylation reduced mTOR stability and was accompanied by decreased AKT Ser473 phosphorylation [23]. In contrast, ZDHHC22 knockdown reduced AKT1 phosphorylation in DCA-exposed gastric epithelial cells in the present study. At the same time, our findings do not exclude indirect regulation through mTOR or other upstream regulators of AKT phosphorylation. Another important finding was the association between ZDHHC22- and palmitoylation-related interventions and mitochondrial redox homeostasis. DCA exposure increased intracellular and mitochondrial ROS signals, reduced the mitochondrial membrane potential, and induced ultrastructural abnormalities, including vacuolization and cristae disruption. Naringenin, AKT inhibition, ZDHHC22 knockdown, and 2-BP treatment each attenuated these abnormalities. Naringenin also preserved mitochondrial ultrastructure in both gastric tissues and GES-1 cells. The similar effects of these interventions support a relationship among AKT signaling, palmitoylation-related regulation, oxidative stress, and mitochondrial dysfunction in DCA-exposed gastric epithelial cells. However, these findings should not be interpreted as evidence that palmitoylation generally impairs mitochondrial function. Previous studies have identified protective palmitoylation-dependent mechanisms, including ABHD10-mediated regulation of the PRDX5 redox system [25] and a

role for ZDHHC13 in mitochondrial function and metabolism [26]. Taken together, these observations emphasize that the effects of protein palmitoylation are highly dependent on the modified substrate and cellular context.

Naringenin has previously been reported to exert antioxidant, anti-inflammatory, and gastroprotective effects [17,18,20,21]. Our findings extend these observations to an experimental model of bile acid-induced gastric metaplastic changes. Importantly, naringenin administration was initiated after four months of DCA exposure, when MUC2 expression was already increased but typical histological features of GIM were not evident in the examined sections. Thus, the intervention began during an early marker-positive state rather than after histologically established GIM. The subsequent reduction in gastric histological alterations and in MUC2 and CDX2 expression is therefore consistent with an early preventive or disease-attenuating effect in this model, rather than reversal of established intestinal metaplasia. This distinction is relevant to the potential translational interpretation of the findings, because an intervention that delays early metaplastic progression may not necessarily reverse more advanced lesions. The concurrent reductions in AKT1 palmitoylation and phosphorylation following naringenin treatment suggest that modulation of these processes may contribute to its protective effects. Transcriptomic analysis further identified ZDHHC22 as a candidate gene associated with the naringenin response. The observed change in ZDHHC22 expression could reflect direct transcriptional regulation, altered mRNA stability, or a secondary response to reduced cellular stress. Naringenin may also exert direct radical-scavenging effects or enhance endogenous antioxidant defenses, including Nrf2-related responses [17,27]. These AKT1-independent mechanisms could act in parallel with the signaling changes observed in the present study. Rescue experiments in which ZDHHC22 activity or AKT1 palmitoylation is selectively restored during naringenin treatment will be needed to determine the extent to which this pathway contributes to naringenin-mediated protection.

To determine whether AKT1 is a direct substrate of ZDHHC22, protein interaction studies will be needed. In addition, the relevant AKT1 cysteine residue or residues were not defined in gastric epithelial cells. Site-specific mutagenesis, combined with appropriately controlled rescue experiments, will be required to determine whether AKT1 palmitoylation directly influences its phosphorylation, subcellular localization, and downstream effects. Furthermore, the short-term induction of MUC2 and CDX2 in GES-1 cells represents a metaplasia-associated molecular phenotype rather than complete intestinal transdifferentiation. Validation in gastric organoids and additional in vivo models will be necessary to determine the generalizability of these findings.

5. Conclusions

DCA exposure increases ZDHHC22-associated AKT1 palmitoylation, accompanied by enhanced AKT1 phosphorylation, metaplasia-associated marker expression, oxidative stress, and mitochondrial abnormalities. Early naringenin intervention attenuated these molecular and phenotypic changes in the experimental models. These findings identify ZDHHC22-associated AKT1 palmitoylation as a previously underexplored regulatory process in bile acid-induced gastric metaplastic responses and provide a basis for further investigation of its mechanistic contribution to naringenin-mediated protection.

Supplementary Materials: The following supporting information can be downloaded at: https://www.mdpi.com/article/10.3390/antiox15121549/s1. Figure S1: Effect of naringenin on the viability of GES-1 cells; Table S1: Antibodies; Table S2 Primer Sequences

Author Contributions: N.C.: Writing—original draft, Data curation, Formal analysis, Project administration, Investigation, Methodology, Visualization. Q.H.: Writing—original draft, Data curation, Formal analysis, Investigation, Visualization. S.X.: Writing—original draft, Data curation, Formal analysis. Z.R.:

Investigation, Validation. P.L.: Investigation, Validation. S.G.: Investigation, Validation. H.G.: Investigation, Validation. M.G.: Investigation, Validation. H.Y.: Investigation, Validation. K.J.: Conceptualization, Project administration, Resources, Software, Writing—review and editing. J.Z.: Conceptualization, Funding acquisition, Project administration, Methodology, Resources, Software, Supervision, Writing—review and editing. All authors have read and agreed to the published version of the manuscript**.**

Funding: This research was funded by the National Key R&D Program of China (2024YFE0104000), the National Natural Science Foundation of China (U25A20135), the Tianjin Health Science and Technology Project (TJWJ2024XK004) and the Excellent Clinical Medicine Talents Program Funded by the People's Government of Hebei Province (No. ZF2026429).

Institutional Review Board Statement: The animal study protocol was approved by the Institutional Review Board of the Institute of Radiation Medicine, Chinese Academy of Medical Sciences and Peking Union Medical College (protocol code IRM/2-IACUC-2407-002,approval date: 20240701).

Informed Consent Statement: Not applicable.

Data Availability Statement: Publicly available datasets were analyzed in this study. This data can be found at: GEO database (accession number GSE134520) https://www.ncbi.nlm.nih.gov/geo/query/acc.cgi?acc=GSE134520 (accessed on 11 March 2025) and TCGA-STAD dataset https://portal.gdc.cancer.gov/projects/TCGA-STAD (accessed on 28 February 2025). The original data presented in the study are openly available in the NCBI Gene Expression Omnibus (GEO) at https://www.ncbi.nlm.nih.gov/geo/query/acc.cgi?acc=GSE355366.

Acknowledgments: We acknowledge Figdraw (www.figdraw.com) for its contribution to generating the Graphical Abstract (Copyright Code: ATSSY6b070).

Conflicts of Interest: The authors declare no conflicts of interest.

Abbreviations

BAs: Bile acids; DCA: deoxycholic acid; CAG: Chronic atrophic gastritis; GC: gastric cancer; GEO: Gene Expression Omnibus; GO: Gene Ontology; IM: intestinal metaplasia; IP-ABE: Immunoprecipitation Combined with Acyl-biotin Exchange; KEGG: Kyoto Encyclopedia of Genes and Genomes; NAG: Non-atrophic gastritis; ROS: Reactive oxygen species; TCGA: The Cancer Genome Atlas; TEM: Transmission electron microscopy; ZDHHC: Zinc finger DHHC-type containing.

References

1. Zhang, L.Y.; Zhang, J.; Li, D.; Liu, Y.; Zhang, D.L.; Liu, C.F.; Wang, N.; Wu, S.R.; Lu, W.Q.; Guo, J.Z.; et al. Bile reflux is an independent risk factor for precancerous gastric lesions and gastric cancer: An observational cross-sectional study. *J. Dig. Dis.* **2021**, *22*, 282–290.
2. Kim, K.S.; Peck, B.C.; Hung, Y.H.; Koch-Laskowski, K.; Wood, L.; Dedhia, P.H.; Spence, J.R.; Seeley, R.J.; Sethupathy, P.; Sandoval, D.A. Vertical sleeve gastrectomy induces enteroendocrine cell differentiation of intestinal stem cells through bile acid signaling. *JCI Insight* **2022**, *7*, e154302.
3. Lund, M.L.; Sorrentino, G.; Egerod, K.L.; Kroone, C.; Mortensen, B.; Knop, F.K.; Reimann, F.; Gribble, F.M.; Drucker, D.J.; de Koning, E.J.P.; et al. L-Cell Differentiation Is Induced by Bile Acids Through GPBAR1 and Paracrine GLP-1 and Serotonin Signaling. *Diabetes* **2020**, *69*, 614–623.
4. Li, M.; Zhang, L.; Chen, C.W. Diverse Roles of Protein Palmitoylation in Cancer Progression, Immunity, Stemness, and Beyond. *Cells* **2023**, *12*, 2209.
5. Wu, Z.; Tan, R.; Zhu, L.; Yao, P.; Hu, Q. Protein S-Palmitoylation and Lung Diseases. *Adv. Exp. Med. Biol.* **2021**, *1304*, 165–186.
6. Liu, L.; Wang, L.; Liu, L.; Qu, X.; Zhao, W.; Ding, J.; Zhao, S.; Xu, B.; Yu, H.; Liu, B.; et al. Acyltransferase zinc finger DHHC-type containing 2 aggravates gastric carcinoma growth by targeting Nrf2 signaling: A mechanism-based multicombination bionic nano-drug therapy. *Redox Biol.* **2024**, *70*, 103051.
7. Fan, X.; Gong, M.; Zhang, S.; Niu, W.; Sun, S.; Yu, H.; Chen, X.; Fang, Z. Blocking Palmitoylation of Apelin Receptor Alleviates Morphine Tolerance in Neuropathic Cancer Pain. *Int. J. Biol. Sci.* **2024**, *20*, 47–60.

8. Plain, F.; Howie, J.; Kennedy, J.; Brown, E.; Shattock, M.J.; Fraser, N.J.; Fuller, W. Control of protein palmitoylation by regulating substrate recruitment to a zDHHC-protein acyltransferase. *Commun. Biol.* **2020**, *3*, 411.
9. Zhou, B.; Hao, Q.; Liang, Y.; Kong, E. Protein palmitoylation in cancer: Molecular functions and therapeutic potential. *Mol. Oncol.* **2023**, *17*, 3–26.
10. Han, Z.; Wu, K.; Shen, H.; Li, C.; Han, S.; Hong, L.; Shi, Y.; Liu, N.; Guo, C.; Xue, Y.; et al. Akt1/protein kinase B alpha is involved in gastric cancer progression and cell proliferation. *Dig. Dis. Sci.* **2008**, *53*, 1801–1810. https://doi.org/10.1007/s10620-007-9824-2.
11. Sun, Z.; Liu, Y.; Deng, H.; Wang, S.; Zhang, J.; Xing, C.; Xu, C. Modified Chaishao Liujunzi Decoction inhibits bile acid-induced gastric intestinal metaplasia: From network prediction to experimental verification. *Aging* **2023**, *15*, 13998–14018.
12. Thirumal Kumar, D.; Jain, N.; Evangeline, J.; Kamaraj, B.; Siva, R.; Zayed, H.; Doss, C.G.P. A computational approach for investigating the mutational landscape of RAC-alpha serine/threonine-protein kinase (AKT1) and screening inhibitors against the oncogenic E17K mutation causing breast cancer. *Comput. Biol. Med.* **2019**, *115*, 103513.
13. Liu, Q.; Wang, Z.; Zhou, X.; Tang, M.; Tan, W.; Sun, T.; Wang, Y.; Deng, Y. miR-485-5p/HSP90 axis blocks Akt1 phosphorylation to suppress osteosarcoma cell proliferation and migration via PI3K/AKT pathway. *J. Physiol. Biochem.* **2020**, *76*, 279–290.
14. Blaustein, M.; Piegari, E.; Martínez Calejman, C.; Vila, A.; Amante, A.; Manese, M.V.; Zeida, A.; Abrami, L.; Veggetti, M.; Guertin, D.A.; et al. Akt Is S-Palmitoylated: A New Layer of Regulation for Akt. *Front. Cell Dev. Biol.* **2021**, *9*, 626404.
15. Bu, L.; Zhang, Z.; Chen, J.; Fan, Y.; Guo, J.; Su, Y.; Wang, H.; Zhang, X.; Wu, X.; Jiang, Q.; et al. High-fat diet promotes liver tumorigenesis via palmitoylation and activation of AKT. *Gut* **2024**, *73*, 1156–1168.
16. Rebello, C.J.; Beyl, R.A.; Lertora, J.; Greenway, F.L.; Ravussin, E.; Ribnicky, D.M.; Poulev, A.; Kennedy, B.J.; Castro, H.F.; Campagna, S.R.; et al. Safety and pharmacokinetics of naringenin: A randomized, controlled, single-ascending-dose clinical trial. *Diabetes Obes. Metab.* **2020**, *22*, 91–98.
17. Ramprasath, T.; Senthamizharasi, M.; Vasudevan, V.; Sasikumar, S.; Yuvaraj, S.; Selvam, G.S. Naringenin confers protection against oxidative stress through upregulation of Nrf2 target genes in cardiomyoblast cells. *J. Physiol. Biochem.* **2014**, *70*, 407–415.
18. Dou, W.; Zhang, J.; Sun, A.; Zhang, E.; Ding, L.; Mukherjee, S.; Wei, X.; Chou, G.; Wang, Z.-T.; Mani, S. Protective effect of naringenin against experimental colitis via suppression of Toll-like receptor 4/NF-κB signalling. *Br. J. Nutr.* **2013**, *110*, 599–608.
19. Zhang, F.; Dong, W.; Zeng, W.; Zhang, L.; Zhang, C.; Qiu, Y.; Wang, L.; Yin, X.; Zhang, C.; Liang, W. Naringenin prevents TGF-β1 secretion from breast cancer and suppresses pulmonary metastasis by inhibiting PKC activation. *Breast Cancer Res.* **2016**, *18*, 38.
20. Wang, K.; Chen, Z.; Huang, L.; Meng, B.; Zhou, X.; Wen, X.; Ren, D. Naringenin reduces oxidative stress and improves mitochondrial dysfunction via activation of the Nrf2/ARE signaling pathway in neurons. *Int. J. Mol. Med.* **2017**, *40*, 1582–1590.
21. Li, W.S.; Lin, S.C.; Chu, C.H.; Chang, Y.-K.; Zhang, X.; Lin, C.-C.; Tung, Y.-T. The Gastroprotective Effect of Naringenin against Ethanol-Induced Gastric Ulcers in Mice through Inhibiting Oxidative and Inflammatory Responses. *Int. J. Mol. Sci.* **2021**, *22*, 11985.
22. Lee, J.H.; Liu, R.; Li, J.; Zhang, C.; Wang, Y.; Cai, Q.; Qian, X.; Xia, Y.; Zheng, Y.; Piao, Y.; et al. Stabilization of phosphofructokinase 1 platelet isoform by AKT promotes tumorigenesis. *Nat. Commun.* **2017**, *8*, 949.
23. Huang, J.; Li, J.; Tang, J.; Wu, Y.; Dai, F.; Yi, Z.; Wang, Y.; Li, Y.; Wu, Y.; Ren, G.; et al ZDHHC22-mediated mTOR palmitoylation restrains breast cancer growth and endocrine therapy resistance. *Int. J. Biol. Sci.* **2022**, *18*, 2833–2850.
24. Tian, L.; McClafferty, H.; Knaus, H.G.; Ruth, P.; Shipston, M.J. Distinct acyl protein transferases and thioesterases control surface expression of calcium-activated potassium channels. *J. Biol. Chem.* **2012**, *287*, 14718–14725.
25. Cao, Y.; Qiu, T.; Kathayat, R.S.; Azizi, S.-A.; Thorne, A.K.; Ahn, D.; Fukata, Y.; Fukata, M.; Rice, P.A.; Dickinson, B.C. ABHD10 is an S-depalmitoylase affecting redox homeostasis through peroxiredoxin-5. *Nat. Chem. Biol.* **2019**, *15*, 1232–1240.
26. Shen, L.F.; Chen, Y.J.; Liu, K.M.; Haddad, A.N.S.; Song, I.-W.; Roan, H.-Y.; Chen, L.-Y.; Yen, J.J.Y.; Chen, Y.-J.; Wu, J.-Y.; et al. Role of S-Palmitoylation by ZDHHC13 in Mitochondrial function and Metabolism in Liver. *Sci. Rep.* **2017**, *7*, 2182.
27. Rashmi, R.; Bojan Magesh, S.; Mohanram Ramkumar, K.; Suryanarayanan, S.; Venkata SubbaRao, M. Antioxidant Potential of Naringenin Helps to Protect Liver Tissue from Streptozotocin-Induced Damage. *Rep. Biochem. Mol. Biol.* **2018**, *7*, 76–84.

Disclaimer/Publisher's Note: The statements, opinions and data contained in all publications are solely those of the individual author(s) and contributor(s) and not of MDPI and/or the editor(s). MDPI and/or the editor(s) disclaim responsibility for any injury to people or property resulting from any ideas, methods, instructions or products referred to in the content.